

# Experimental realization of optical eigenmode super-resolution

Kevin Piché\*,<sup>1</sup> Jonathan Leach,<sup>1</sup> Allan S. Johnson,<sup>1</sup> Jeff Z. Salvail,<sup>1</sup>  
Mikhail I. Kolobov,<sup>2</sup> and Robert W. Boyd<sup>1,3</sup>

<sup>1</sup>Department of Physics, University of Ottawa, Ottawa, Ontario, Canada

<sup>2</sup>Laboratoire PhLAM, Université de Lille 1, F-59655 Villeneuve d'Ascq Cedex, France

<sup>3</sup>Institute of Optics, University of Rochester, Rochester, New York, 14627, USA

\*[kpich049@uottawa.ca](mailto:kpich049@uottawa.ca)

**Abstract:** We experimentally demonstrate the feasibility of a super-resolution technique based on eigenmode decomposition. This technique has been proposed theoretically but, to the best of our knowledge, has not previously been realized experimentally for optical imaging systems with circular apertures. We use a standard diffraction-limited  $4f$  imaging system with circular apertures for which the radial eigenmodes are the circular prolate spheroidal functions. For three original objects with different content of angular information we achieve 45%, 49%, and 89% improvement of resolution over the Rayleigh limit. The work presented can be considered as progress towards the goal of reaching the quantum limits of super-resolution.

© 2012 Optical Society of America

**OCIS codes:** (050.1940) Diffraction; (100.3020) Image reconstruction-restoration.

---

## References and links

1. P. Kok, A. N. Boto, D. S. Abrams, C. P. Williams, S. L. Braunstein, and J. P. Dowling, "Quantum-interferometric optical lithography: towards arbitrary two-dimensional patterns," *Phys. Rev. A* **63**, 063407 (2001).
2. H. Shin, K. W. C. Chan, H. J. Chang, and R. W. Boyd, "Quantum spatial superresolution by optical centroid measurements," *Phys. Rev. Lett.* **107**, 083603 (2011).
3. R. W. Boyd and J. P. Dowling, "Quantum lithography: status of the field," *Quant. Inf. Processing* **11**, 891–901 (2012).
4. G. Toraldo Di Francia, "Resolving power and information," *J. Opt. Soc. Am.* **45**, 497–501 (1955).
5. J. L. Harris, "Diffraction and resolving power," *J. Opt. Soc. Am.* **54**, 931–936 (1964).
6. Z. Liu, H. Lee, Y. Xiong, C. Sun, and X. Zhang, "Far-field optical hyperlens magnifying sub-diffraction-limited objects," *Science* **315**, 1686 (2007).
7. J. B. Pendry, "Negative refraction makes a perfect lens," *Phys. Rev. Lett.* **85**, 3966–3969 (2000).
8. D. R. Smith, "How to build a superlens," *Science* **308**, 502–503 (2005).
9. N. Fang, H. Lee, C. Sun, and X. Zhang, "Sub-diffraction-limited optical imaging with a silver superlens," *Science* **308**, 534–537 (2005).
10. E. T. F. Rogers, J. Lindberg, T. Roy, S. Savo, J. E. Chad, M. R. Dennis, and N. I. Zheludev, "A super-oscillatory lens optical microscope for subwavelength imaging," *Nat. Materials* **11**, 432–435 (2012).
11. V. Giovannetti, S. Lloyd, L. Maccone, and J. H. Shapiro, "Sub-rayleigh-diffraction-bound quantum imaging," *Phys. Rev. A* **79**, 013827 (2009).
12. F. Guerrieri, L. Maccone, F. N. C. Wong, J. H. Shapiro, S. Tisa, and F. Zappa, "Sub-rayleigh imaging via N-photon detection," *Phys. Rev. Lett.* **105**, 163602 (2010).
13. C. K. Rushforth, "Restoration, resolution, and noise," *J. Opt. Soc. Am.* **58**, 539–545 (1968).
14. G. Toraldo Di Francia, "Degrees of freedom of an image," *J. Opt. Soc. Am.* **59**, 799–804 (1969).
15. M. Bertero and E. R. Pike, "Resolution in diffraction-limited imaging, a singular value analysis," *Opt. Acta* **29**, 727–746 (1982).

16. A. C. D. Luca, S. Kosmeier, K. Dholakia, and M. Mazilu, "Optical eigenmode imaging," *Phys. Rev. A* **84**, 021803 (2011).
17. M. I. Kolobov and C. Fabre, "Quantum limits on optical resolution," *Phys. Rev. Lett.* **85**(18), 3789–3792 (2000).
18. I. V. Sokolov and M. I. Kolobov, "Squeezed-light source for superresolving microscopy," *Opt. Lett.* **29**, 703–705 (2004).
19. V. N. Beskrovnyy and M. I. Kolobov, "Quantum limits of super-resolution in reconstruction of optical objects," *Phys. Rev. A* **71**(4), 043802 (2005).
20. V. N. Beskrovnyy and M. I. Kolobov, "Quantum theory of super-resolution for optical systems with circular apertures," *Opt. Commun.* **264**(1), 9–12 (2006).
21. V. N. Beskrovnyy and M. I. Kolobov, "Quantum-statistical analysis of superresolution for optical systems with circular symmetry," *Phys. Rev. A* **78**(4), 043824 (2008).
22. D. Slepian, "Prolate spheroidal wave functions, Fourier analysis and uncertainty IV," *Bell Syst. Tech. J.* **43**, 3009–3057 (1964).
23. I. C. Moore and M. Cada, "Prolate spheroidal wave functions, an introduction to the Slepian series and its properties," *Appl. Comput. Harmon. Anal.* **16**, 208–230 (2004).
24. G. Walter and T. Soleski, "A new friendly method of computing prolate spheroidal wave functions and wavelets," *Appl. Comput. Harmon. Anal.* **19**, 432–443 (2005).
25. H. Xiao, V. Rokhlin, and N. Yarvin, "Prolate spheroidal wavefunctions, quadrature and interpolation," *IOP-Science* **17**, 805–838 (2000).
26. D. Slepian and E. Sonnenblick, "Eigenvalues associated with prolate spheroidal wave functions of zero order," *Bell Syst. Tech. J.* **44**, 1745–1759 (1965).
27. B. R. Frieden, "Band-unlimited reconstruction of optical objects and spectra," *J. Opt. Soc. Am.* **57**, 1013–1019 (1967).
28. B. R. Frieden, "Evaluation, design and extrapolation methods for optical signals, based on use of the prolate functions," *Prog. Opt.* **9**, 311–407 (1971).
29. C.-S. Hu, "Prolate spheroidal wave functions of large frequency parameters  $c = kf$  and their applications in electromagnetic theory," *IEEE Trans. Antennas Propag.* **AP-34**, 114–119 (1986).
30. J. C. Heurtley, "Hyperspheroidal functions-optical resonators with circular mirrors," *Proc. Symp. Quasi-Opt.* **1**, 367–375 (1964).

## 1. Introduction

One of the fundamental limits to the resolution of an optical imaging system is the diffraction of light. Diffraction, together with finite-aperture optics, results in a loss of high spatial frequency information contained in the original object. The loss of this information results in a final image that is blurred, and fine details present in the original object can no longer be resolved.

As a guide, the resolving power of an optical system can be estimated from the Rayleigh criterion, which gives an approximate limit to the conditions where two point sources can be distinguished. The spatial resolution of a lens with a focal length  $f$  and diameter  $D$  is given by

$$1.22 \frac{f\lambda}{D}, \quad (1)$$

where  $\lambda$  is the wavelength of the light. It is well known that this diffraction limit can be overcome in certain circumstances. Super-resolution imaging is the field of research dedicated to resolving details in images to a higher precision than that given by the Rayleigh criterion. As super-resolution imaging has many applications in many disciplines, numerous techniques have been developed for this purpose. In addition super-resolution techniques play an important role in lithography [1–3].

The loss of information in an imaging system can be quantified with the use of the fact that the number of degrees-of-freedom of an object can differ from that of the image-forming instrument [4]. The number of degrees-of-freedom of an image and the detection of ambiguous images were introduced as key concepts for the resolution limits of imaging. If two distinct objects have identical images after propagating through the optical system, these two objects cannot be distinguished without the use of *a priori* information. The identical images after propagation are ambiguous images. It was later shown that, in certain optical systems, objects

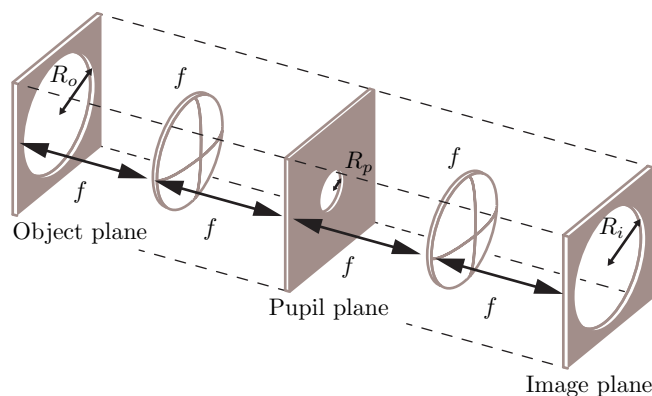


Fig. 1. Schematic of the  $4f$  optical system used for eigenmode super-resolution imaging. The two lenses both have a focal length of  $f$ , and the distance between every plane and subsequent lens is  $f$ . The object plane has an aperture of radius  $R_o$ , the pupil plane has an aperture of radius  $R_p$ , and the image plane has an aperture of radius  $R_i = R_o$ .

with a finite size do not have ambiguous images [5]. Resolution in these systems is only limited by noise given that the image can be accurately measured.

The discussion of super-resolution was initiated in the middle of the last century. It is well known that (i) super-resolution is in principle possible, given some amount of *a priori* information about the object, and (ii) the degree of super-resolution is determined by the signal-to-noise ratio (SNR) in the detection scheme; however, there are many unanswered questions. Indeed, new techniques for achieving super-resolution have recently appeared in the literature such as hyperlenses [6], negative refraction lenses [7–9], super-oscillating lenses [10] and photon-counting techniques [11, 12]. Several key issues of super-resolution remain to be clarified such as, for example, the relation between the amount of a priori information and the degree of super-resolution. Recent work has addressed the question about super-resolution of sparse objects using the technique of compressed sensing. Still largely unaddressed at the experiment level are the ultimate limits of super-resolution imposed by the quantum nature of the light. The inevitable quantum fluctuations result in the so-called standard quantum limit of photodetection.

Another approach to super-resolution imaging is based on the optical eigenmodes of a system [13–15]. Eigenmodes are complex fields that propagate through the optical system with an unchanged spatial distribution and a known attenuation in amplitude [16]. In this case, the improvement to the resolution is limited by the achievable signal-to-noise ratio of the transmitted eigenmodes. Recently, in-depth theoretical studies into the effects of quantum fluctuations on eigenmode super-resolution imaging have been performed for the case of one-dimensional and two-dimensional images [17–21]. We are motivated by the goal of reaching the quantum limit of super-resolution so that we can measure the degree of super-resolution as a function of the SNR. The work presented in this paper is a first step towards this goal.

In this work, we present the first demonstration of eigenmode super-resolution with prolate spheroidal modes. The prolate spheroidal modes are the optical eigenmodes of a diffraction-limited  $4f$  system with circular apertures. We find that in certain cases we are able to reconstruct images with a resolution beyond the Rayleigh criterion of our optical setup.

## 2. Theory

The optical system that we consider is a diffraction-limited  $4f$  imaging system; see Fig. 1. In such a system, we assume that the original diffraction-free image is contained within the radius  $R_o$  at the object plane. This image is optically Fourier transformed by the first lens onto the pupil plane where there is a pupil aperture of radius  $R_p$ . It is at this plane that the high spatial frequency modes are absorbed. The remainder of the field is Fourier transformed by the second lens onto the image plane, resulting in a final image that is diffraction-limited.

The eigenmodes of the  $4f$  system are prolate spheroidal modes [22]. These are modes with circular symmetry that are attenuated by a factor of  $\lambda_{\ell p}$  on propagation through the optical system, where  $\ell$  and  $p$  are angular and radial indices respectively. The attenuation factor is the eigenvalue of its corresponding eigenmode and ranges from 0, which corresponds to no transmission, to 1, which corresponds to full transmission.

Due to the circular symmetry of the  $4f$  system, it is convenient to use polar coordinates  $r$  and  $\theta$ . Many authors use the dimensionless coordinates  $r/R_o$  in the definition of the prolate spheroidal modes. However, we choose to use the dimensional variable  $r$ , such that the prolate spheroidal modes range from 0 to  $R_o$ . A prolate spheroidal mode is defined as

$$\Phi_{\ell p} = \varphi_{\ell p}(r, c)e^{-i\ell\theta}, \quad (2)$$

where  $\varphi_{\ell p}$  is a generalised prolate spheroidal function, and  $c$  is the space-bandwidth product. The space-bandwidth product of the  $4f$  system is given by

$$c = 2\pi \frac{R_o R_p}{\lambda f}, \quad (3)$$

where  $\lambda$  is the wavelength,  $f$  is the focal length of the lenses,  $R_o$  is the radius of the image, and  $R_p$  is the radius of the pupil aperture [21]. The space-bandwidth product is a measure of how much information can be transmitted through the optical system and provides a rough estimate of the number of degrees of freedom of the optical system.

The generalised prolate spheroidal functions  $\varphi_{\ell p}$ , which are of considerable interest in both mathematics [23–26] and physics [27–29], were independently developed by Slepian [22] and Heurley [30]. As the generalised prolate spheroidal functions are difficult to calculate analytically, we take the approach detailed in Ref. [21] to generate them numerically. In summary, the numerical procedure entails writing the function as a series of radial Zernike polynomials. These polynomials are weighted by coefficients that are given by a three-term recurrence relation. Figure 2 illustrates the intensity and phase profiles of selected prolate spheroidal modes.

The prolate spheroidal modes form a complete orthogonal basis over a disc of radius  $R_o$ . The corresponding orthogonality relation is

$$\int_0^{2\pi} \int_0^{R_o} \Phi_{\ell p} \Phi_{\ell' p'}^* r dr d\theta = 2\pi \delta_{\ell\ell'} \delta_{pp'}. \quad (4)$$

Thus, the complex fields at the object and image planes, denoted  $A(r, \theta)$  and  $B(r, \theta)$  respectively, can be written as superpositions of prolate spheroidal modes using the following equations:

$$A(r, \theta) = \sum_{\ell=-\infty}^{\infty} \sum_{p=0}^{\infty} \alpha_{\ell p} \Phi_{\ell p}, \quad (5)$$

and

$$B(r, \theta) = \sum_{\ell=-\infty}^{\infty} \sum_{p=0}^{\infty} \beta_{\ell p} \Phi_{\ell p}. \quad (6)$$

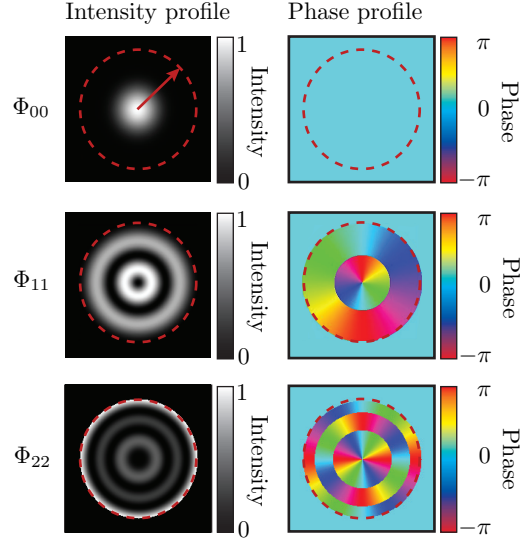


Fig. 2. Normalized intensity and phase profiles of three different prolate spheroidal modes. The dashed red circles indicate the area in which the images are contained. The red arrow indicates  $R_o$ .

The images at the object and image planes are given by  $|A(r, \theta)|^2$  and  $|B(r, \theta)|^2$  respectively. The complex coefficients  $\alpha_{\ell p}$  and  $\beta_{\ell p}$  are obtained by the following complex overlap integrals:

$$\alpha_{\ell p} = \frac{1}{2\pi} \int_0^{2\pi} \int_0^{R_o} A(r, \theta) \Phi_{\ell p}^* r dr d\theta, \quad (7)$$

and

$$\beta_{\ell p} = \frac{1}{2\pi} \int_0^{2\pi} \int_0^{R_o} B(r, \theta) \Phi_{\ell p}^* r dr d\theta. \quad (8)$$

As the prolate spheroidal modes are the orthogonal eigenmodes of the  $4f$  system, there is a straightforward relationship between the coefficients  $\alpha_{\ell p}$  and  $\beta_{\ell p}$ . Let the linear operator  $S$  represent the transmission of an image through the  $4f$  system. Applying the operator  $S$  to the complex field at the object plane results in the complex field at the image plane,

$$S[A(r, \theta)] = B(r, \theta). \quad (9)$$

Each prolate spheroidal mode  $\Phi_{\ell p}$  is attenuated by a factor of  $\lambda_{\ell p}$  on propagation through the  $4f$  system; see Fig. 3(a). In terms of the operator  $S$ ,

$$S[\Phi_{\ell p}] = \lambda_{\ell p} \Phi_{\ell p}. \quad (10)$$

This is the familiar eigenvalue problem. For the detailed procedure used to calculate the eigenvalues  $\lambda_{\ell p}$  numerically, see Ref. [21]. The eigenvalues of a subset of the prolate spheroidal modes that correspond to a  $4f$  system with  $c = 10$  are illustrated in Fig. 3(b).

Equation (9) expanded in terms of the prolate spheroidal modes is equal to

$$\sum_{\ell, p} \alpha_{\ell p} S[\Phi_{\ell p}] = \sum_{\ell, p} \alpha_{\ell p} \lambda_{\ell p} \Phi_{\ell p} = \sum_{\ell, p} \beta_{\ell p} \Phi_{\ell p}. \quad (11)$$

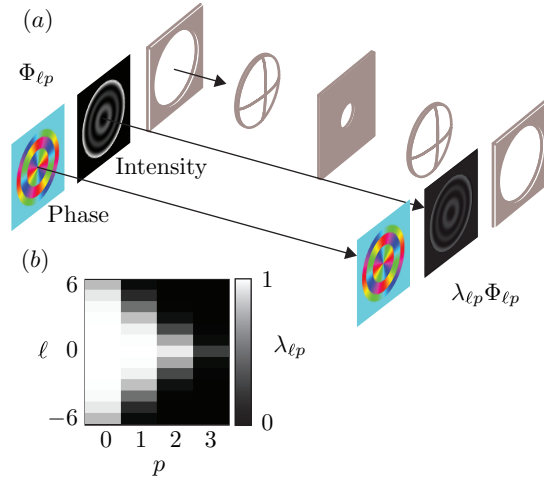


Fig. 3. (a) Transmission of prolate spheroidal modes through a  $4f$  system. The intensity and phase profile for the  $\Phi_{22}$  mode are shown. On propagation through the  $4f$  system, the mode  $\Phi_{22}$  becomes  $\lambda_{22}\Phi_{22}$ . (b) Subset of eigenvalues  $\lambda_{\ell p}$  for the  $4f$  system with  $c = 10$ .

It follows that the coefficients of the modes  $\alpha_{\ell p}$  that are required to reconstruct the field at the object plane can be calculated by measuring the coefficients of the modes  $\beta_{\ell p}$  at the image plane and dividing by the anticipated transmission  $\lambda_{\ell p}$ ,

$$\alpha_{\ell p} = \frac{\beta_{\ell p}}{\lambda_{\ell p}}. \quad (12)$$

Substituting Eq. (12) into Eq. (5), we find that a reconstruction of the original image can be found by taking the modulus squared of the sum over all different prolate spheroidal modes,

$$|C(r, \theta)|^2 = \left| \sum_{\ell=-\infty}^{\infty} \sum_{p=0}^{\infty} \frac{\beta_{\ell p}}{\lambda_{\ell p}} \Phi_{\ell p} \right|^2. \quad (13)$$

In the case of zero noise and perfect reconstruction, the reconstructed image  $|C(r, \theta)|^2$  is the same as the original image  $|A(r, \theta)|^2$ . We now see how super-resolution can be performed with knowledge of the complex decomposition coefficients in the image plane and the corresponding eigenmodes of the system. In practice, the gains in resolution are limited by the signal-to-noise levels of the attenuated modes. Therefore, the number of modes that are used for image reconstruction is finite.

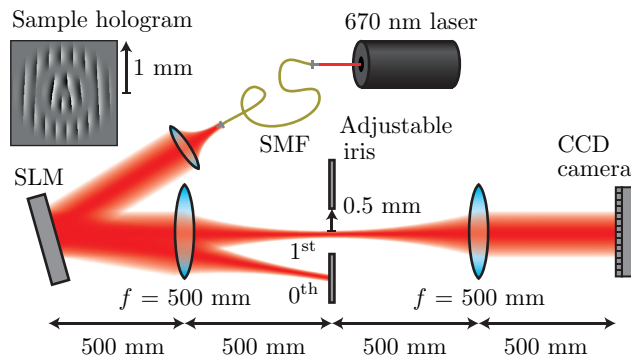


Fig. 4. Schematic of the experimental setup.

### 3. Experiment

A detailed summary of our experimental procedure follows. We generate a coherent superposition of prolate spheroidal modes using a spatial light modulator (SLM, Holoeye Pluto) placed in the object plane of the  $4f$  system; see Fig. 4 for details. The SLM is illuminated with light from a spatially-filtered 670 nm diode laser that is expanded to a beam waist of  $\sim 1$  cm. The first diffraction order of the reflected light off the SLM propagates through a  $4f$  system constructed of two lenses of focal lengths  $f = 0.5$  m, an adjustable iris placed at the focal point of each lens, and a standard CCD camera (Dalsa Genie). The iris absorbs the high spatial frequency components of the light field such that the image recorded by the camera is diffraction-limited. The space-bandwidth product  $c$  of the system is set by adjusting the radius of the iris  $R_p$  and the radius of the image  $R_o$  on the SLM. For the purpose of the experiment, the space-bandwidth product is set to  $c \approx 10$ .

The intensity profile of the superposition of prolate spheroidal modes generated by the SLM, which is in the object plane, constitutes the original diffraction-free image. The intensity profile of the light recorded by the camera, which is in the image plane, constitutes the observed diffraction-limited image. By applying the super-resolution technique, we are able to reconstruct an estimate of the original image.

A key requirement of the eigenmode super-resolution technique is the knowledge of the complex field  $B(r, \theta)$  at the image plane. To achieve this, we first interfere a reference mode  $E_{\text{ref}}(r, \theta)$  with the received field and record the intensity distribution of the interference pattern with the camera  $I(r, \theta)$ . Second, we shift the phase of the reference by  $2\pi/N$ , where  $N$  is an integer greater than 3, and record the new interference pattern. This process is repeated such that the phase of the reference is shifted through  $2\pi$ , and the field can be recovered using

$$B(r, \theta) = \frac{1}{N} \sum_{q=0}^{N-1} e^{i2\pi q/N} I_q(r, \theta), \quad (14)$$

where the  $q^{\text{th}}$  intensity distribution recorded by the camera  $I_q(r, \theta)$  is equal to  $|E_{\text{ref}}(r, \theta) \exp(-i2\pi q/N) + B(r, \theta)|^2$  [16]. After the field  $B(r, \theta)$  at the object plane is recovered, the complex coefficients  $\beta_{\ell p}$  are established by decomposing over the appropriate prolate spheroidal modes using Eq. (8). An estimate of the original image is then reconstructed using Eq. (13).

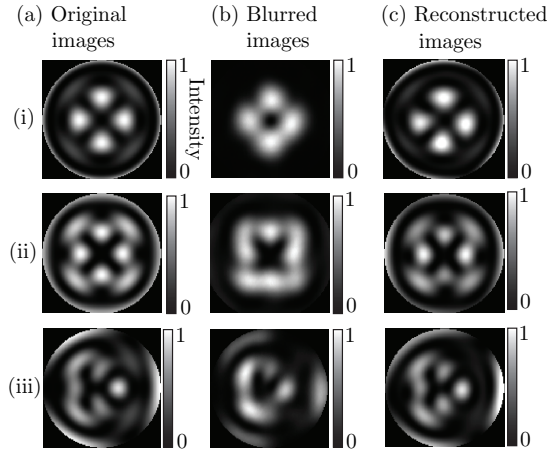


Fig. 5. Experimental results of eigenmode super-resolution. (a) The original images that were propagated through the system. (b) The recorded diffracted-limited images. (c) The super-resolved images. The images are contained within a 1 mm radius.

#### 4. Results and discussion

We performed eigenmode super-resolution imaging for a range of initial superpositions of  $\Phi_{\ell p}$  modes; Fig. 5 shows the original images, the experimentally recorded diffraction-limited images, and the super-resolved images following the reconstruction procedure. By comparison of each column, it is clear that the super-resolved images closely resemble the original images, whereas the experimentally recorded images are subject to loss and blurring.

The modulus squared of the  $\Phi_{\ell p}$  mode coefficients, which are normalized such that the maximum value is equal to one, are shown in Fig. 6. It can be seen from this figure that the high-order modes of the images are attenuated in the diffraction-limited image; but they are recovered when the coefficients are divided by  $\lambda_{\ell p}$ .

The gains in resolution can be quantified by comparing the complex overlaps of the reconstructed fields and diffraction-limited fields with respect to the original fields. The ratios of the modulus squared of these quantities gives an indicator of the super-resolution factors. We define the complex overlap of a super-resolved complex field and an original complex field as

$$\kappa = \int_0^{2\pi} \int_0^{R_o} A(r, \theta) C^*(r, \theta) r dr d\theta; \quad (15)$$

and the complex overlap of a diffraction-limited complex field and an original complex field  $\eta$  is similarly defined with  $B(r, \theta)$  replacing  $C(r, \theta)$ . The super-resolution factor is then defined by

$$\left| \frac{\kappa}{\eta} \right|^2 - 1. \quad (16)$$

The super-resolution factors for the three images in Fig. 5 are (i) 89%, (ii) 49%, and (iii) 45%.

The eigenmode super-resolution technique is applicable to any diffraction-limited optical system when a set of orthogonal eigenmodes that forms a complete basis over the object and image planes can be determined. If a complete orthogonal eigenmode basis can be found, all initial images can be distinguished after post-processing.

It should be noted that for high-order modes the eigenvalues  $\lambda_{\ell p}$  tend to zero. The decomposition coefficients  $\beta_{\ell p}$  are therefore divided by small numbers and any noise will be amplified and

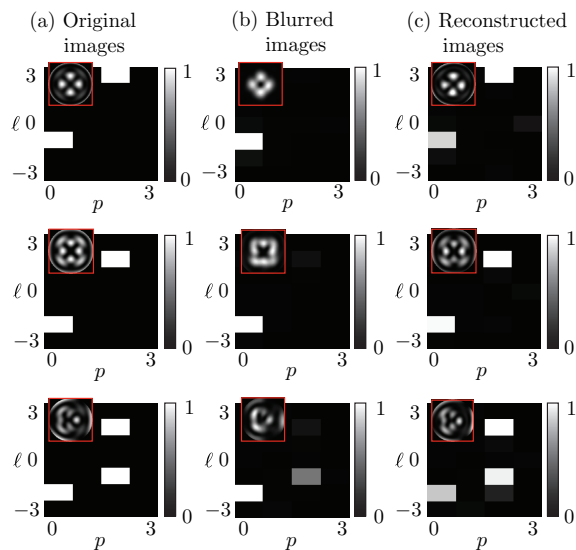


Fig. 6. The normalised modulus squared of the decomposition coefficients of the images in Fig. 5. The insets indicate the appropriate image at each stage.

introduce errors into the estimation of the original coefficients. Consequently, there is a limit on the degree of super-resolution that is achievable in practice, and it is important to choose an appropriate range of values for  $\ell$  and  $p$  for the reconstruction. If too many coefficients are included, noise becomes the dominating factor; if too few coefficients are included, there will be no improvement in the resolution of the reconstructed image compared to the recorded one. A threshold for  $\lambda_{\ell p}$  is thus required for the reconstruction. This threshold can be set as the inverse of the signal-to-noise ratio [21]. In our experiment, we set the threshold so that modes with eigenvalues greater than 0.05 are included, and those with eigenvalues less than 0.05 are not. We find that this limit gives a good balance between the super-resolution gained and the noise introduced.

## 5. Conclusion

In conclusion, we report the first experimental realization of eigenmode super-resolution imaging for the case of a diffraction-limited  $4f$  system with circular apertures. The quantum limits of super-resolution are most easily addressed in the framework that we present; thus, this work represents important progress towards investigating this regime.

The limitations of the technique that we report are that we require knowledge of the optical eigenmodes of the system, which is not a trivial task for more complex imaging schemes, and that the complex field recovery process adds additional time to the reconstruction procedure. However, these limitations can be overcome as the eigenmodes of an arbitrary system can be found through experimental characterization, and similarly, the field recovery time can be reduced with alternative interferometric implementations.

The technique is general, in that it can be applied to other systems where the optical eigen-

modes can be established. The improvement to the resolution of the final reconstructed image is related to the maximum achievable signal-to-noise ratio of the experiment. Future research will focus on the resolution limits that are set by the quantum fluctuations of the light field [20,21].

### **Acknowledgments**

We would like to thank F. Stef Roux and Claude Fabre for their contributions to this paper. This work was supported by the Canada Excellence Research Chairs (CERC) Program.